Atmospheric deterioration of Qin brick in an environmental chamber at Emperor Qin's Terracotta Museum, China

T.F. Hu [a,b,c,*], S.C. Lee [c], J.J. Cao [a,b], W.K. Ho [c], K.F. Ho [c], J.C. Chow [b,d], J.G. Watson [b,d], B. Rong [e], Z.S. An [b]

[a] Department of Environmental Science and Engineering, Xi'an Jiaotong University, Xi'an, China
[b] SKLLQG, Institute of Earth Environment, Chinese Academy of Sciences, Xi'an, China
[c] Department of Civil and Structural Engineering, The Hong Kong Polytechnic University, Hong Kong, China
[d] Division of Atmospheric Sciences, Desert Research Institute, Reno, NV, USA
[e] Emperor Qin's Terracotta Warriors and Horses Museum, Xi'an, China

ARTICLE INFO

ABSTRACT

Potential mechanisms for the changing appearance of Qin terracotta was evaluated on simulated bricks with, SO_2, NH_3, O_3, and a NH_3/O_3 mixture for total dosages of 2.2–5.4 ppm-years. Changes in the surface composition and appearance were evaluated with scanning electron microscopy/energy dispersive X-ray analysis (SEM–EDX) and X-ray photoelectron spectroscopy (XPS). No observable changes with O_3 exposure were found. Sulfate as sulfur and ammonium as nitrogen increased by 1.2 at% and 0.8 at% of the surface deposit as determined by XPS. O_3 did not have a detectable effect by itself, but when combined with NH_3, NO_3 as nitrogen increased by 1.5 at%, indicating a strong oxidation of NH_3 to nitric acid. The combination of outdoor O_3 infiltration with indoor NH_3, presumably from the visitors, appears to have a greater potential for damage than either pollutant by itself. SEM–EDX mapping of the surface showed sulfur associated with calcium and magnesium compounds after SO_2 exposure, but not before. More detailed microscopic examination showed this primarily in the form of gypsum, especially near cracks and pits in the surface. Both of these mechanisms are probably among the causes of changes in terracotta appearances since they were unearthed in 1974.

1. Introduction

The discovery of the terracotta warriors and horses of the Qin Dynasty (221–206 BC) in 1974 was one of the most important archeological findings of the 20th century. Today Emperor Qin's Terracotta Warriors reside inside China's largest on-site museum with more than two million visitors each year. The museum is located ∼30 km east of Xi'an, a city of eight million people with increasing traffic, high coal consumption, and intensive construction. The museum is surrounded by agricultural fields in which biomass burning and suspended dust are prominent. Elevated atmospheric pollutant concentrations inside and outside of the museum may contribute to observed changes in appearance of the historical ceramics since their excavation more than 30 years ago.

The floors between rammed earth walls in all the three Pits are paved with rectangular Qin bricks of a fresh orange color that have changed in appearance since being unearthed (Fig. 1). Several studies have been conducted on atmospheric damages to historical ceramics (e.g. Elert et al., 2003; Lopez-Arce et al., 2003; Cardiano et al., 2004; Cultrone et al., 2000, 2005; Lopez-Arce and Garcia-Guinea, 2005; Böke et al., 2006) showing different damage patterns that depend on the materials and the type of pollution.

This study investigates morphological and chemical changes on the surfaces of bricks created by the same materials and methods used by the original builders. These simulated bricks are exposed to gaseous pollutants in an environmental chamber. Scanning electron microscopy with energy dispersive X-ray analysis (SEM–EDX) detects changes in the surface morphology and elemental distributions on the brick surfaces, while X-ray photoelectron spectroscopy (XPS) reveals chemical changes to the brick surface.

2. Methodology

2.1. Sample preparation

Previous mineralogical and Mössbauer studies have identified the local Lishan clay as the raw material of the Qin brick and

* Corresponding author. Department of Environmental Science and Engineering, Xi'an Jiaotong University, No. 28, Xianning West Road, Xi'an 710049, China. Tel.: +86 29 8266 8385; fax: +86 29 8266 8789.
E-mail address: hutafeng@hotmail.com (T.F. Hu).

Fig. 1. Photograph of the archaeological site, showing the terracotta statues arranged in the passageways between rammed earth walls. All the floors were paved with rectangular Qin bricks (size: $280 \times 140 \times 70$ mm^3).

Table 1
Chemical composition of the surface and inner parts of the Qin bricks (Zhang, 1998).

(wt.%)	SiO$_2$	Al$_2$O$_3$	CaO	Fe$_2$O$_3$	MgO	K$_2$O	Na$_2$O	TiO$_2$
Surface	63.66	17.74	2.61	6.72	2.62	3.05	1.24	0.81
Core	63.72	17.43	2.96	6.88	2.62	3.41	1.33	0.81

terracotta, fired at temperature between 950 and 1000 °C. The difference between terracotta and Qin brick is that terracotta was fired under reducing conditions (Zhang, 1998; Zhao et al., 2002; Hsia and Huang, 2003). As shown in Table 1, the chemical composition is homogeneous, as indicated by measurements on the surface of and within the bricks. The X-ray diffraction (XRD) patterns suggest that the mineralogical composition of Qin brick is primarily quartz (70%) and feldspar (15%), with minor muscovite, biotite, and hematite. The higher percentage of quartz in the Qin bricks (70%) relative to that in the Pit No. 1 soil (<45%) reflects the composition of fine sand that was added to prevent cracking during manufacture (Zhang, 1998).

The simulated brick was prepared using 70% clay soil from Pit No. 2 and 30% fine quartz sand (20–30 μm), molded into $50 \times 20 \times 15$ mm^3 blocks, and fired for 8 h at 950–1000 °C in an electric oven. After cooling for 2 days, $10 \times 10 \times 2$ mm^3 sections were cut with a diamond saw for placement in the exposure chamber.

2.2. Experimental chamber

The experimental setup is shown in Fig. 2. The test chamber consists of two 2.4 L stainless-steel cylindrical compartments. The interior surfaces are passivated by electropolishing and Teflon connection lines are used to minimize pollutant absorption and desorption from the inner surfaces. Laboratory air used for purging is maintained at 23 ± 2 °C through the laboratory environmental controls and relative humidity is maintained at $50 \pm 5\%$ by a humidification chamber. As shown in Table 2, these temperatures and relative humidity are typical of those measured in Pit No. 1 Exhibition Hall (Pit 1) (Zhang, 1998; Cao et al., 2004). Once sealed, the sample is kept in the dark to isolate the effects of pollutant exposure from possible photochemical degradation of the material.

Four separate exposures were tested over 100 day periods for: 1) 8 ppm sulfur dioxide (SO$_2$), 2) 10 ppm ammonia (NH$_3$), 3) 20 ppm ozone (O$_3$), and 4) 10 ppm NH$_3$ with 20 ppm O$_3$. These concentration levels are 400–800 times higher than averages measured in Pit 1 (Table 2) and provide worst-case exposure situations. Pollutant dosage is the product of concentration and exposure duration (ASHRAE, 2003; Tétreault, 2003), corresponding to a 100–200 year exposure for Pit 1.

Before each test, the chamber system was conditioned with the gas mixture for at least 24 h. The flow rate through the chamber was
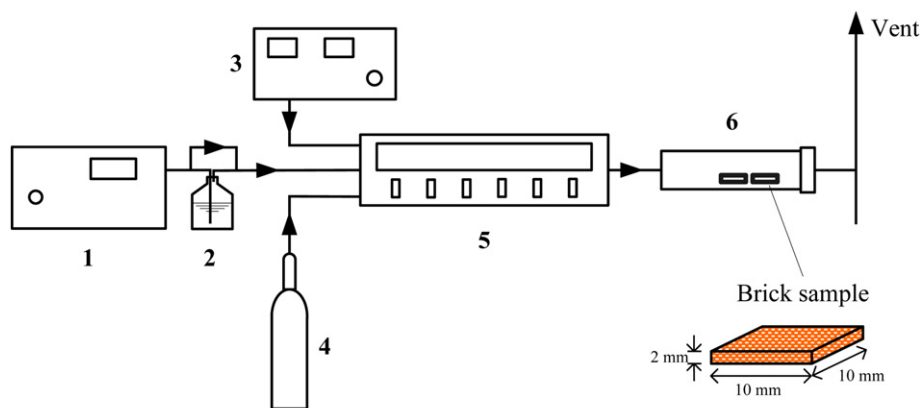
1. Zero air generator (Thermo Environmental Inc., Model 111, Franklin, MA, USA)
2. Humidification chamber (50±5%)
3. Ozone generator (Prominent International Company, PIE Ozonation, HK)
4. Standard gas (1,000ppm SO$_2$ Bal. N$_2$; 1000ppm NH$_3$ Bal. N$_2$)
5. Mass flow calibrator (Advanced Pollution Instrumentation Inc., Model 700, San Diego, CA, USA)
6. Environmental micro-chamber (2.4 L stainless-steel)

Fig. 2. Schematic diagram of the experimental setup for environmental exposure tests.

Table 2
Records of indoor environment inside Pit No. 1 exhibition hall of the Museum.

Monitoring date	Annual avg. temperature (°C)	Annual avg. RH (%)	Avg. SO_2 (ppb)[a]	Avg. NH_3 (ppb)[a]	Avg. O_3 (ppb)[b]
Apr/2006–Apr/2007	19.6	49.6	9.6 ± 4.2	26.8 ± 20.8	43.9 ± 27.7
Aug/2004	26.2	70.8	–	–	–
1993	–	–	12.4 ± 11.7	–	–
1992	13.7	67	–	–	–
1989	13.8	68	–	–	–
Chamber test in this study	23 ± 2	50	8000	10,000	20,000
Equivalent exposure period (yr)	–	–	202	102	125

–: Not available.
 [a] Daily data were collected over 24 h every 6th days by gas-absorbing measurements, $n = 56$.
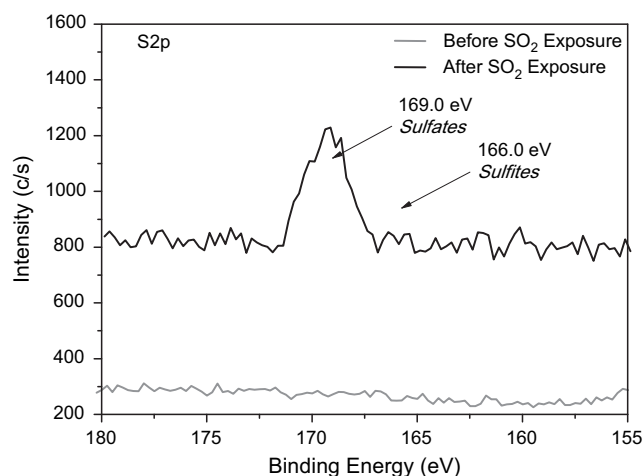 [b] Data were collected once every 5 min by an ozone monitor (2B Technologies, Inc. Model 202, Boulder, CO, USA) from 1 Oct to 7 Oct 2006, $n = 2016$.

1.5 L min^{-1}. The concentration levels were monitored every 3 days at the outlet of the chamber system during the test. Control samples were sealed in plastic cassettes and stored in the laboratory.
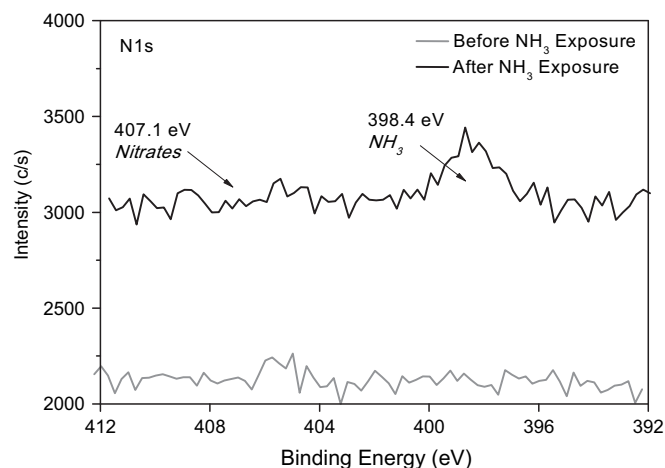
2.3. Sample analysis

Before and after exposure, the chemical states of specific element (S, O, and N) on the surfaces of the bricks were evaluated by XPS (PHI Quantum 2000, Eden Prairie, MN, USA) with a monochromatic Al $K\alpha$ source and a charge neutralizer (Gardella, 1989). Binding energies were referenced to the C 1s peak at 284.8 eV of the surface adventitious carbon. Relative atomic percentages (at%) for each element was calculated from peak areas.

For SEM analysis, the samples were mounted on aluminum stubs with conductive adhesive tape and coated with carbon under vacuum (Danilatos, 1991). For each sample, secondary electron images were acquired using a JSM-6460 LV scanning electron microscope (Japan Electron Optics Laboratory Co. Ltd., Tokyo, Japan), with a 20 kV accelerating voltage at a work distance of 10 mm. Elemental X-ray mapping of selected areas on the central part of the brick surfaces was performed with a Si–Li EDX detector with an ultrathin window (Thermo Electron Corporation, Noran System SIX, Franklin, MA, USA). The X-ray peak intensities for each element were converted into relative atomic percentages using the EDX software without ZAF correction.

3. Results and discussion

3.1. XPS analysis

High-resolution scans of the S 2p peak from the brick's surface brick before and after SO_2 exposure are shown in Fig. 3. The relative concentration of elemental S increased from <0.1 at% before SO_2 exposure to 1.2 at% after exposure. A new sulfur peak with a binding energy of 169.0 eV shows the presence of sulfates on the post-exposure brick surface. Sulfation can proceed in two ways during calcareous stone and mortar decay (Sabbioni, 2000; Lopez-Arce and Garcia-Guinea, 2005; Giavarini et al., 2008): 1) SO_2 adsorbed onto the wet surface reacts with calcium carbonate ($CaCO_3$) to form calcium sulfite ($CaSO_3$), which is then further oxidized to calcium sulfate ($CaSO_4$); or 2) SO_2 oxidizes to H_2SO_4 in the aqueous phase, either on the material surface or in the air, and subsequently attacks the carbonate, leading to the formation of a gypsum crust. The sulfur peak corresponding to sulfite, with a binding energy between 165.5 and 167.5 eV, is not apparent in the

Fig. 4. High-resolution X-ray photoelectron spectroscopy (XPS) spectra of the N 1s region before and after NH_3 exposure.

Fig. 3. High-resolution X-ray photoelectron spectroscopy (XPS) spectra of the S 2p region before and after SO_2 exposure.
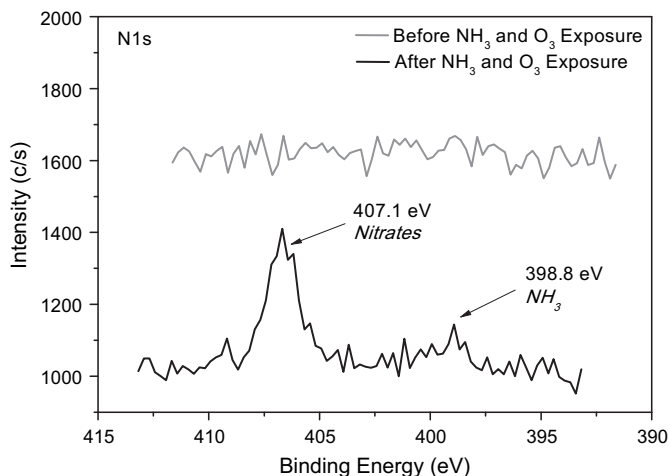
Fig. 5. High-resolution X-ray photoelectron spectroscopy (XPS) spectra of the N 1s region before and after NH_3/O_3 exposure.

Table 3
Atomic fraction (at%) of elements detected by Energy dispersive X-ray analysis (EDX) on the surface of the Qin brick before and after purging with SO_2 gas.

at%	Na	Mg	Al	Si	S	K	Ca	Ti	Fe
Before purging	1.7 ± 0.1	2.5 ± 0.4	11.9 ± 1.0	44.9 ± 2.5	–	3.7 ± 0.3	21.4 ± 1.8	0.7 ± 0.2	10.1 ± 0.2
After purging	1.9 ± 0.2	3.1 ± 0.6	12.8 ± 0.9	44.6 ± 2.1	4.3 ± 1.7	3.8 ± 0.8	19.6 ± 1.7	0.8 ± 0.2	9.0 ± 0.5

–: Not detectable.

XPS spectra, implying sulfate formation on brick surface by the second pathway, or a depletion of sulfite as an intermediate in the process of sulfation.

Fig. 4 shows XPS spectra for the N 1s region before and after NH_3 exposure; The new N peak at ∼398.8 eV corresponds to NH_3 and the surface abundance of N increased from <0.1 at% to 0.8 at% for the exposed surface.

O_3 is a highly oxidizing gas that has adversely affected various museum collections, including paper, pigment, rubber and poly-meric materials (Brimblecombe, 1990; Cass et al., 1991; Morrison and Nazaroff, 2002). In this study, no obvious change in the elemental composition or chemical state was observed in response to O_3 exposure without other pollutants. However, changes were found for the NH_3 and O_3 mixture, as indicated by the 407.1 eV N 1s nitrate peak in Fig. 5. O_3 apparently oxidizes the NH_3 to NO_3, probably in the form of nitric acid (HNO_3). Elemental N increased from <0.1 at% to 1.5 at% after exposure to the mixture, nearly twice the N increase observed for NH_3 alone. O_3 enhances NO and NO_2 oxidation to NO_3 in the aqueous phase (Johnson et al., 1996; Massey, 1999), but low (50 or 100 ppb) O_3 concentrations were not previously found to react with NH_3 (Weschler, 2000). In this study with a much higher O_3 concen-tration, the NH_4 peak with pure NH_3 was replaced by an NO_3 peak, indicating that the NH_3 was oxidized to an acidic species that has been previously shown to damage stone surfaces (Sikiotis and Kirkitsos, 1995).

3.2. SEM–EDX analysis

Average atomic abundances from SEM surface scans before and after SO_2 exposure are shown in Table 3. Small changes are observed for all elements except sulfur, which was enriched from negligible amounts to 4.3 at% after exposure. This value is higher than the XPS result of 1.2 at% because C and O peaks are not included in the EDX spectra to avoid any interference from the carbon coating. Elemental K, Ti, and Fe peaks were found in the EDX spectra, but these were not detected by the XPS analysis, because the EDX electron beam analyzes the top 500–5000 nm of the sample surface, much deeper than the penetration of the XPS photoelectron measurement (about 5–10 nm).
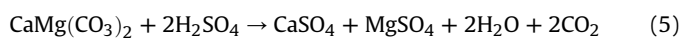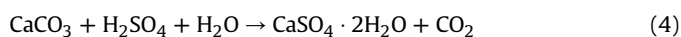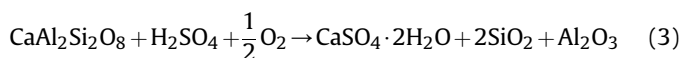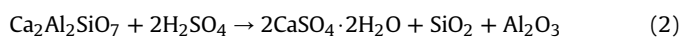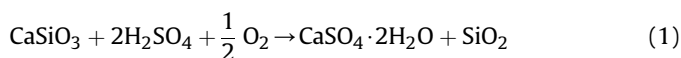
The raw materials used in the manufacture of Qin bricks contain calcite and dolomite (Wen, 1989; Zhang, 1998). Surface X-ray mappings of S, Ca, and/or Mg after SO_2 exposure (Fig. 6) show inhomogeneous interactions between atmospheric SO_2 and the calcite ($CaCO_3$) and dolomite ($CaMg(CO_3)_2$) components in the brick material, yielding calcium sulfate ($CaSO_4$) and magnesium sulfate ($MgSO_4$) products. Sulfates are enriched on specific Ca-rich and Mg-rich particles. Other than at these points of enrichment,
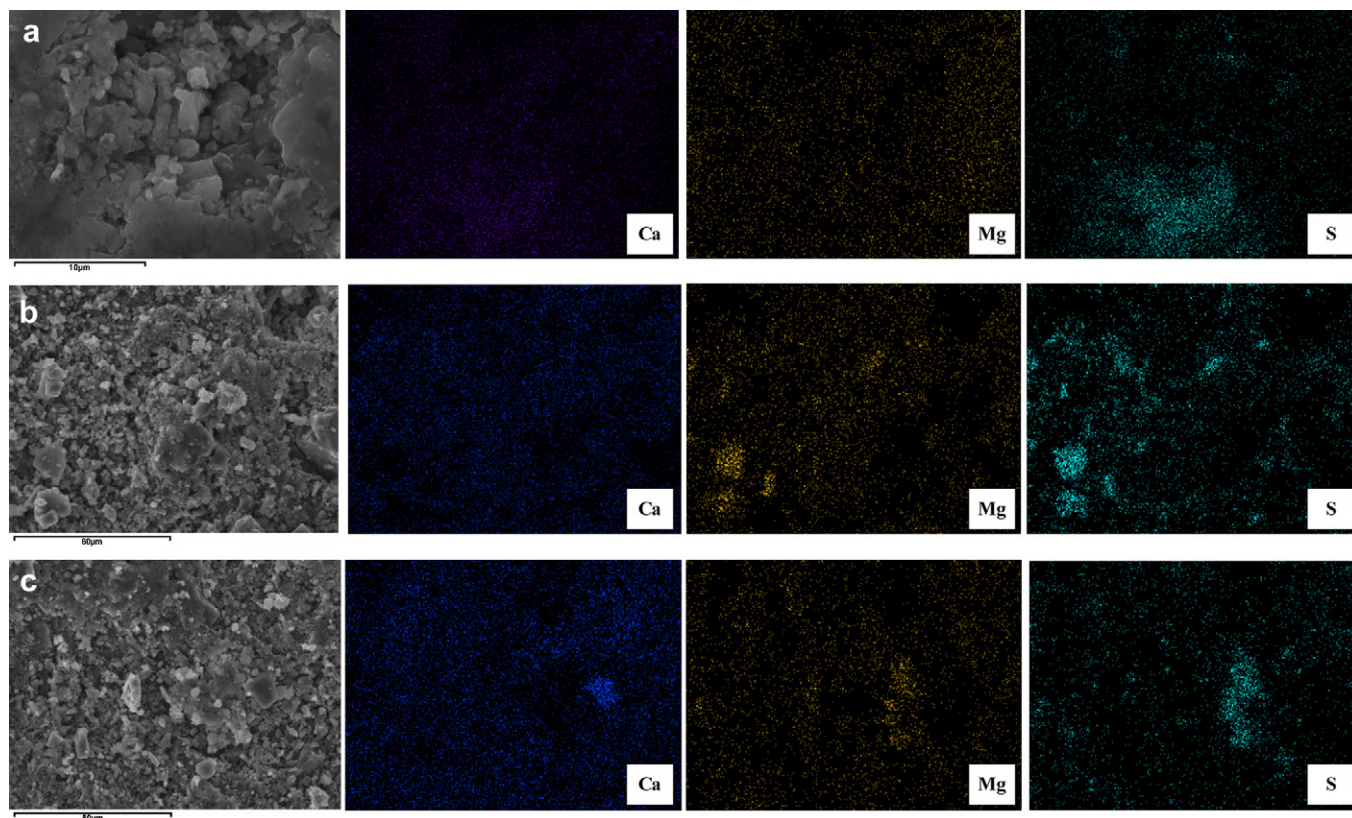
Fig. 6. Scanning electron micrographs and X-ray elemental mapping after SO_2 exposure. S is found at the same locations as (a) Ca, magnification 5000×; (b) Mg, magnification 1000×; (c) Ca and Mg, magnification 1000×.

elemental S was uniformly distributed on the brick surface at a lower density, as shown by the light spots.

Black crusts on historic buildings have been association with atmospheric SO_2 pollution in industrialized and urban areas (Camuffo et al., 1982; Sabbioni et al., 1998; Giavarini et al., 2008). Reaction of Ca-rich silicates in sulfuric acid is a well-known phenomenon (Cultrone et al., 2000; Sabbioni et al., 2001; Simão et al., 2006). Cultrone et al. (2000) observed sulfated crusts forming over a 24-h period in the presence of 400 ppm SO_2. The crust even formed on silicate-rich substrates with low calcite content (<10 wt%). Sulfuric acid (H_2SO_4) generated by catalytic oxidation of SO_2 attacks calcium-bearing surfaces containing wollastonite ($CaSiO_3$), gehlenite ($Ca_2Al_2SiO_7$), and Ca–feldspars ($CaAl_2Si_2O_8$), resulting in the formation of gypsum crystals. Therefore, the following sulfation reactions may take place on the surfaces of Qin bricks:

$$CaSiO_3 + 2H_2SO_4 + \frac{1}{2}O_2 \rightarrow CaSO_4 \cdot 2H_2O + SiO_2 \tag{1}$$

$$Ca_2Al_2SiO_7 + 2H_2SO_4 \rightarrow 2CaSO_4 \cdot 2H_2O + SiO_2 + Al_2O_3 \tag{2}$$

$$CaAl_2Si_2O_8 + H_2SO_4 + \frac{1}{2}O_2 \rightarrow CaSO_4 \cdot 2H_2O + 2SiO_2 + Al_2O_3 \tag{3}$$

$$CaCO_3 + H_2SO_4 + H_2O \rightarrow CaSO_4 \cdot 2H_2O + CO_2 \tag{4}$$

$$CaMg(CO_3)_2 + 2H_2SO_4 \rightarrow CaSO_4 + MgSO_4 + 2H_2O + 2CO_2 \tag{5}$$

Soluble salts have been related to building materials such as rocks (Benavente et al., 2007), limestone and marble (Cardell et al., 2003), bricks (Cultrone et al., 2005), ceramics, and concrete (Marinoni et al., 2003). Gypsum crystal formation was observed in close proximity to fly ash and anchored the fly ash to the limestone surface (Ausset et al., 1999). Weathering tests have also shown chemical deterioration from gypsum on artisanal glass (Carmona et al., 2005). Surface crusting and damage may be enhanced by trapped particulate matter and water uptake due to its hygroscopic properties (Gonçalves et al., 2006).

Hu et al. (2006) detected gypsum in Pit 1 air and sealer flakes from the Terracotta warriors. According to the records between 1989 and 1992, the daily average temperature fluctuated from −4.2 °C to 32 °C in Pit No. 1, with daily average RH from 35% to 92% (Zhang, 1998). Under the conditions of temperature and relative humidity inside the Qin Museum, the crystallization, dissolution, penetration into cracks, and recrystallization of gypsum particles played an important part in changing the appearance of the statues.

4. Conclusions

Atmospherically induced corrosion of Qin bricks in response to SO_2, NH_3, O_3, and $NH_3 + O_3$ exposures equivalent to 2.2–5.4 ppm-years was evident after residence in an exposure chamber with subsequent XPS and SEM–EDX analysis. Sulfate as sulfur and ammonium as nitrogen increased by 1.2% and 0.8% of the surface deposit as determined by XPS. O_3 did not have a detectable effect by itself, but when combined with NH_3, NO_3 as nitrogen increased by 1.5%, indicating a strong oxidation of NH_3 to nitric acid. The combination of outdoor O_3 infiltration with indoor NH_3, presumably from the visitors, appears to have a greater potential for damage than either pollutant by itself.

SEM–EDX mapping of the surface showed sulfur associated with calcium and magnesium compounds after SO_2 exposure, but not before. More detailed microscopic examination showed this primarily in the form of gypsum, especially near cracks and pits in the surface. Both of these mechanisms are probably among the causes of changes in terracotta appearances since they were unearthed in 1974.

Embryonic soluble salt particles on the noncompact and porous surface increase the risk of salt weathering and the formation of black crust. In Pit No. 1 exhibition hall of the Museum, the free exchange of the air mass through the open windows provides excellent natural ventilation. The aggressive indoor environment, including fluctuations in temperature and humidity and the infiltration of pollutant gases into the building, plays an important role in the potential chemical and subsequent physical weathering risk. This analysis has revealed the detailed chemical transformation of Qin bricks and clarifies the chemistry of their surfaces, which will be useful in selecting appropriate indoor air-quality controls, including mechanical ventilation, filtration system, and microclimate control measures, to reduce the indoor concentrations of gaseous pollutants and the fluctuations in temperature and humidity.

References

Am. Soc. Heat. Refrig. Air-Cond. Eng. (ASHRAE), 2003. Risk Management Guidance for Health, Safety and Environmental Security under Extraordinary Incidents. ASHRAE, Atlanta, GA. Report.

Ausset, P., Del Monte, M., Lefèvre, R.A., 1999. Embryonic sulphated black crusts on carbonate rocks in atmospheric simulation chamber and in the field: role of carbonaceous fly-ash. Atmospheric Environment 33, 1525–1534.

Benavente, D., Martínez-Martíneza, J., Cuetoa, N., García-del-Cura, M.A., 2007. Salt weathering in dual-porosity building dolostones. Engineering Geology 94, 215–226.

Böke, H., Akkurt, S., İpekoğlu, B., Uğurlu, E., 2006. Characteristics of brick used as aggregate in historic brick–lime mortars and plasters. Cement and Concrete Research 36, 1115–1122.

Brimblecombe, P., 1990. The composition of museum atmospheres. Atmospheric Environment 24B, 1–8.

Camuffo, D., Del Monte, M., Sabbioni, C., 1982. Wetting deterioration and visual features of stone surfaces in an urban area. Atmospheric Environment 16, 2253–2259.

Cao, J.J., Rong, B., Lee, S.C., Chow, J.C., Ho, K.F., Liu, S.X., Zhu, C.S., 2004. Composition of indoor aerosols at Emperor Qin's Terra-cotta Museum, Xi'an, China, during summer. China Particuology 2005 (3), 170–175.

Cardell, C., Delalieux, F., Roumpopoulos, K., Moropoulou, A., Auger, F., Van Grieken, R., 2003. Salt-induced decay in calcareous stone monuments and building in a marine environment in SW France. Construction and Building Materials 17, 165–179.

Cardiano, P., Ioppolo, S., De Stefano, C., Pettignano, A., Sergi, S., Piraino, P., 2004. Study and characterization of the ancient bricks of monastery of "San Filippo di Fragalà" in Frazzanò (Sicily). Analytica Chimica Acta 519, 103–111.

Carmona, N., Villegas, M.A., Fernández Navarro, J.M., 2005. Corrosion behaviour of R_2O–CaO–SiO_2 glasses submitted to accelerated weathering. Journal of the European Ceramic Society 25, 903–910.

Cultrone, G., De La Torre, M.J., Sebastian, E.M., Cazalla, O., Rodriguez-Navarro, C., 2000. Behavior of brick samples in aggressive environments. Water, Air, and Soil Pollution 119, 191–207.

Cultrone, G., Sidraba, I., Sebastián, E., 2005. Mineralogical and physical characterization of the bricks used in the construction of the "Triangul Bastion", Riga (Latvia). Applied Clay Science 28, 297–308.

Cass, G.R., Nazaroff, W.W., Tiller, C., Whitmore, P.M., 1991. Protection of works of art from damage due to atmospheric ozone. Atmospheric Environment 25A, 441–451.

Danilatos, G.D., 1991. Review and outline of environmental SEM at present. Journal of Microscopy 6, 391–402.

Elert, K., Cultrone, G., Navarro, C.R., Pardo, E.S., 2003. Durability of bricks used in the conservation of historic buildings – influence of composition and microstructure. Journal of Cultural Heritage 4, 91–99.

Gardella Jr., J.A., 1989. Recent developments in instrumentation for x-ray photoelectron spectroscopy. Analytical Chemistry 61, 589–600.

Giavarini, C., Santarelli, M.L., Natalini, R., Freddi, F., 2008. A non-linear model of sulphation of porous stones: numerical simulations and preliminary laboratory assessments. Journal of Cultural Heritage 9, 14–22.

Gonçalves, T.D., Rodrigues, J.D., Abreu, M.M., 2006. Evaluating the salt content of salt-contaminated samples on the basis of their hygroscopic behaviour: Part II: experiments with nine common soluble salts. Journal of Cultural Heritage 7, 193–200.

Hsia, Y., Huang, H., 2003. Mössbauer studies in Chinese archaeology. Hyperfine Interaction 150, 33–50.

Hu, T.F., Li, X.X., Dong, J.G., Rong, B., Shen, Z.X., Cao, J.J., Lee, S.C., Chow, J.C., Watson, J.G., 2006. Morphology and elemental composition of dustfall particles inside Emperor Qin's Terra-cotta Warriors and Horses Museum. China Particuology 4, 346–351.

Johnson, J.B., Montgomery, M., Thompson, G.E., Wood, G.C., Sage, P.W., Cooke, M.J., 1996. The influence of combustion-derived pollutants on limestone deterioration: 1. The dry deposition of pollutant gases. Corrosion Science 38, 105–131.

Lopez-Arce, P., Garcia-Guinea, J., 2005. Weathering traces in ancient bricks from historic buildings. Building and Environment 40, 929–941.

Lopez-Arce, P., Garcia-Guinea, J., Fierro, J.L.G., 2003. Manganese micro-nodules on ancient brick walls. Science of the Total Environment 302, 267–274.

Marinoni, N., Birelli, M.P., Rostagno, C., Pavese, A., 2003. The effects of atmospheric multipollutants on modern concrete. Atmospheric Environment 37, 4701–4712.

Massey, S.W., 1999. The effects of ozone and NO_X on the deterioration of calcareous stone. Science of the Total Environment 227, 109–121.

Morrison, G.C., Nazaroff, W.W., 2002. Ozone interactions with carpet: secondary emissions of aldehydes. Environmental Science and Technology 36, 2185–2192.

Sabbioni, C., 2000. Multipollutants: evidence in stone and mortar decay. In: Protection and Conservation of the Cultural Heritage of the Mediterranean Cities. Fifth International Symposium on the Conservation of Monuments in the Mediterranean Basin, Seville, pp. 15–16.

Sabbioni, C., Zappia, G., Ghedini, N., Gobbi, G., Favoni, O., 1998. Black crust on ancient mortars. Atmospheric Environment 32, 215–223.

Sabbioni, C., Zappia, G., Riontino, C., Blanco-Varela, M.T., Aguilera, J., Puertas, F., Van Balen, K., Toumbakari, E.E., 2001. Atmospheric deterioration of ancient and modern hydraulic mortars. Atmospheric Environment 35, 539–548.

Sikiotis, D., Kirkitsos, P., 1995. The adverse effects of nitrates on stone monuments. Science of the Total Environment 171, 173–182.

Simão, J., Ruiz-Agudo, E., Rodriguez-Navarro, C., 2006. Effects of particulate matter from gasoline and diesel vehicle exhaust emissions on silicate stone sulfation. Atmospheric Environment 40, 6905–6917.

Tétreault, J., 2003. Airborne Pollutants in Museums, Galleries and Archives: Risk Assessment, Control Strategies and Preservation Management. Canadian Conservation Institute, Ottaway, ON.

Wen, Q.Z., 1989. Chinese Loess Geochemistry. Science Press, Beijing (in Chinese).

Weschler, C.J., 2000. Ozone in indoor environments: concentration and chemistry. Indoor Air 10, 269–288.

Zhang, Z.J., 1998. Study on Conservation of Qin Terra-cotta Army. Shaanxi People Education Press, Xi'an (in Chinese).

Zhao, W., Xu, A., Li, R., Gao, Z., Li, G., Xie, J., Han, G., Feng, S., Fan, D., Zhang, Y., Cai, Z., Zhang, Z., Zhu, J., 2002. Microelement analysis of source of raw materials of terracotta warriors and horses of Qin's Mausoleum in pits No. 1 and No. 2. Chinese Science Bulletin 47, 1337–1340.